Section 4

Parameterization of important atmospheric and surface processes, effects of different parameterizations

Evaluation of the Stable Boundary Layer processes in the Global Environmental Multiscale (GEM) Model over the Arctic Ocean during SHEBA

Pierre-Luc Carpentier, Colin Jones
CRCMD, University of Quebec at Montreal
Contact : carpentier.pierre-luc@sca.uqam.ca

1. Introduction

Coupled Global Climate Models (CGCMs) participating in the Phase 2 of the Coupled Model Intercomparison Project (CMIP2) simulate poorly the projected Arctic amplification of climate change near the surface over the Arctic ocean (e.g. Holland and Bitz, 2003). Also, Tjernström *et al.* (2004) report that climate models participating in the Arctic regional climate model intercomparison project (ARCMIP) represent poorly the stably stratified Arctic boundary layer surface turbulent fluxes of heat, momentum and moisture that couple the lower atmosphere with the ice-covered Arctic Ocean. The first goal of this research is to evaluate the GEM model simulated near-surface climate and turbulent processes by comparing them to those observed during the Surface Heat Budget of the Arctic Ocean (SHEBA) year. The second goal of this study is to evaluate the sensitivity of GEM simulations to stability functions and roughness length parameterizations.

2. Model experiment

A simulation was made with GEM on a limited area grid of 70x80 grid boxes centered at a longitude of 156 °W and a latitude of 67 °N with a horizontal resolution of 0.5 degree. 53 vertical levels are used with the top of the model located at 10 hPa. The model integration began in September 1996 and ended in October 1998 with a 30 minutes time step. A spin-up period of one year was included before comparing GEM with the SHEBA observations (Persson *et al.*, 2002) that started in October 1997 and ended a year later. Lateral boundary conditions were supplied from ERA-40 at every 6 hours and the surface boundary conditions of ice fraction and sea-surface temperature (SST) were prescribed from the AMIP II data set. It is worth mentioning that the surface skin temperature distribution was obtained from a surface heat budget computation and wasn't prescribed from the Advanced Very High Resolution Radiometer (AVHRR) used by Tjernström *et al.* (2004) in order to give more degrees of freedom to the model.

3. Results

Comparisons of simulated near-surface state variables with SHEBA observations are shown in Figures 1(a) to (c). The surface wind comparison (Figure 1(a)) suggests large errors occur under calm conditions, with GEM systematically overestimating the wind speed by an average of 1.14 m/s for all conditions observed during the SHEBA year. Surface air temperature and specific humidity (Figures 1(b) and 1(c) respectively) are reasonably well simulated considering that surface temperature wasn't prescribed in the model. Temperature errors are lower in summer as they are constrained around 0 °C during the melting season. The GEM model has an overall warm bias of 0.53 °C in comparison with SHEBA observations.

The comparison of simulated surface turbulent fluxes with SHEBA observations (Figures 1(d) to (f)) showed that like most of the ARCMIP models, GEM overestimates the friction velocity (momentum flux) with a bias of 0.066 m/s for all conditions and the largest errors during calm conditions. Large errors are found for the simulated sensible and latent heat fluxes. The observed mean sensible heat flux is -1.92 W/m^2 while the mean simulated flux is -1.59 W/m^2. The latent heat flux is largely overestimated (bias of 4.03 W/m^2) in the GEM model like in most of the ARCMIP models. Even if the sensible heat flux amplitude is small compared with the other components of the surface heat budget, such errors could be affecting the low-level cloud cover by transporting moisture upward and, indirectly, affecting the radiative budget at the surface.

3. Summary and discussion

In order to understand the origin of modelling errors and possibly to improve the representation of the

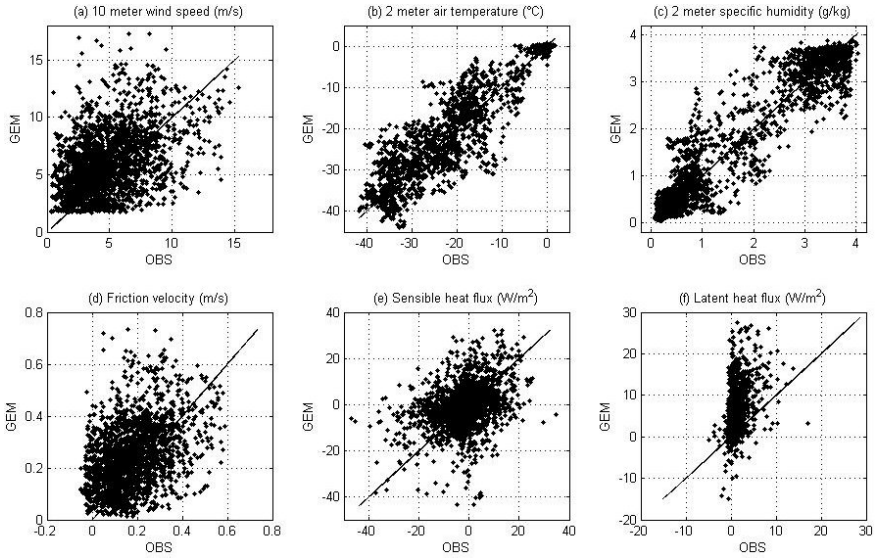

FIG. 1 – Scatter plots of observed (horizontal axis) versus modelled (vertical axis) near-surface (a) wind, (b) air temperature, (c) specific humidity and surface turbulent fluxes of (d) momentum (friction velocity), (e) sensible heat and (f) latent heat. The scatter plots are based on 3 hourly mean time series for the October 29^{th} 1997-October 1^{st} 1998 period. Positive fluxes of sensible and latent heat are in the upward direction and friction velocity is equal to the square root of the surface turbulent flux of momentum.

interaction between the atmosphere and the ice-covered Arctic Ocean, parameterisation of turbulent processes must be evaluated in more detail. GEM and most of the ARCMIP models use a surface layer scheme similar to the well-known Louis (1979) scheme based on Monin-Obukhov similarity theory with surface fluxes of momentum, heat and moisture computed by the generic formula $\overline{w'\chi'}_s = -C_\beta V_s(\overline{\chi}_{ref} - \overline{\chi}_s)$ where χ is u, v, q_v or θ the potential temperature, C_β is the transfer coefficient for χ, V_s is the average 10 meter wind speed, $\overline{\chi}_{ref} - \overline{\chi}_s$ is the average vertical gradient of χ (where β is m, h or v for momentum, heat and moisture respectively) between the surface and a reference level. In this formulation, the transfer coefficient depends on roughness length $z_{0\beta}$. In GEM, roughness lengths are prescribed to a constant value of 0.16 mm for momentum (z_{0m}), heat (z_{0h}) and moisture (z_{0v}) over sea-ice. The transfer coefficients depend also on a stability function ϕ_β that depends on the gradient Richardson number Ri with $\phi_m = 1 + \alpha Ri$ in the stable regime and $\alpha = 12$ (Delage, 1997). The stability function for heat and moisture is calculated by $\phi_h = Pr_t \phi_m$ where Pr_t is the turbulent Prandtl number (equal to one by default in GEM). The sensitivity of GEM to different parameterizations of $z_{0\beta}$, Pr_t and α will be evaluated in future work. Analysis of observations of Prandtl and Richardson number made by the Atmospheric Surface Flux Group (ASFG) (Grachev *et al.*, 2008) during the SHEBA year and associated observations of the stability functions ϕ_β could allow us to improve the quality of the simulations once the sensitivity is to those parameters is established.

4. References

1. Delage, Y., 1997 : Parameterising sub-grid scale vertical transport in atmospheric models under statically stable conditions. *Boundary-Layer Meteorol.*, 82 : 23-48.

2. Grachev, A., et. al., 2008 : Turbulent measurements in the stable atmospheric boundary layer during SHEBA : ten years after. *Acta Geophysica*, vol. 56, no. 1., 142-166.

3. Holland, M. M., Bitz, C. M., 2003 : Polar amplification of climate change in coupled models. *Clim. Dyn.*, 21 : 221-232.

4. Persson, P. Ola G., et al., 2002 : Measurements near the Atmospheric Surface Flux Group tower at SHEBA : Near-surface conditions and surface energy budget. *J. Geophys. Res.*, 107(C10), 8045.

5. Tjernström, M., et al., 2004 : Modelling the arctic boundary layer : an evaluation of six arcmip regional-scale models using data from the SHEBA project. *Boundary-Layer Meteorol.*, 117 : 337-381.

SIMULATION OF ARCTIC MIXED-PHASE CLOUDS OBSERVED DURING M-PACE USING THE GLOBAL ENVIRONMENTAL MULTISCALE MODEL (GEM): EVALUATION OF TWO BULK MICROPHYSICS SCHEMES

Johanne Dorais, Eric Girard, and Ping Du
Department of Earth and Atmospheric Sciences, UQAM, Montreal, Qc.
dorais@sca.uqam.ca

State-of-the-art regional climate models are currently unable to properly simulate cloud-radiation interactions over the Arctic. One of the main challenges is to properly simulate cloud microphysical properties. Cloud thermodynamic phase seems to be particularly important in the magnitude of the cloud radiative forcing (CRF). For instance, Shupe et al. (2006) have shown that CRF can reach 40 W m^{-2} when liquid is present as opposed to 10 W m^{-2} for ice clouds. This research aims at evaluating two bulk microphysics schemes currently used in the Global Environmental Multiscale (GEM) Model. The main objective is to assess the ability of each scheme to properly simulate the partitioning of liquid and ice in mixed-phase clouds and the ability to simulate cloud persistence (in spite of the colloidal instability of the mixed-phase). The first evaluated microphysics scheme is from Sundqvist (1978) (hereafter SUN). The total water content is the only prognostic equation of this scheme. A function depending on temperature is used to discriminate between liquid and ice phases. The second microphysics scheme is from Kong and Yau (1997) (hereafter KY). It is a single-moment scheme with 4 prognostic variables: rain, cloud water, graupel and ice water (which include both cloud ice and snow). The number concentration of ice particle is determined using an empirical relationship, which depends on ice supersaturation only. Further, ice nucleation is not allowed at temperatures above -5^0C.

Short simulations of 36 hours including 12h spin-up are performed over the North Slope of Alaska on a small domain of 447.5 km by 137.5 km covering Barrow, Oliktok and Atqasuk, which are the 3 sites where in-situ and ground-based measurements were taken during the Mixed-Phase Arctic Cloud Experiment (M-PACE) on October 2004. A first simulation at 10 km horizontal resolution is performed over a large domain. This first simulation is then used to drive a 2.5 km horizontal resolution simulation over a smaller domain. Clouds observed on October 5th, 6th, 8th, 9th, 10th and 12th have been simulated. The first 4 days were characterized by relatively high in-cloud temperatures (-11^0C to -6^0C) (hereafter warm regime) while the two last days were colder with in-cloud temperatures down to -17^0C (hereafter cold regime).

Results were first compared with in-situ measurements for each day. Figure 1 shows an example of the vertical profiles of IWC and LWC measured by the aircraft and modeled on October 8th. A mixed-phase stratus cloud was present at 1000 m with a dissipating cloud above. Results show that both schemes capture the vertical structure and the persistence of the cloud. Although the mixed-phase is captured by both schemes, the partitioning between liquid and ice differs significantly when compared to observations as illustrated on Figure 1 for October 8. When all the 6 cases are gathered, it is found that SUN has a systematic negative cloud liquid water bias and a positive cloud water ice bias for all cases examined (see Table 1). It seems that the phase partitioning function of SUN is not appropriate for these Arctic stratus clouds. KY behaves differently depending on temperature. Indeed, for warmer in-cloud cases, it has a positive cloud liquid water bias and a negative cloud ice water bias. On the other hand, KY biases are substantially reduced for colder clouds (see Table 1). This bias could be related to the formulation of the scheme, which restricts the ice nucleation at temperatures below -5^0C.

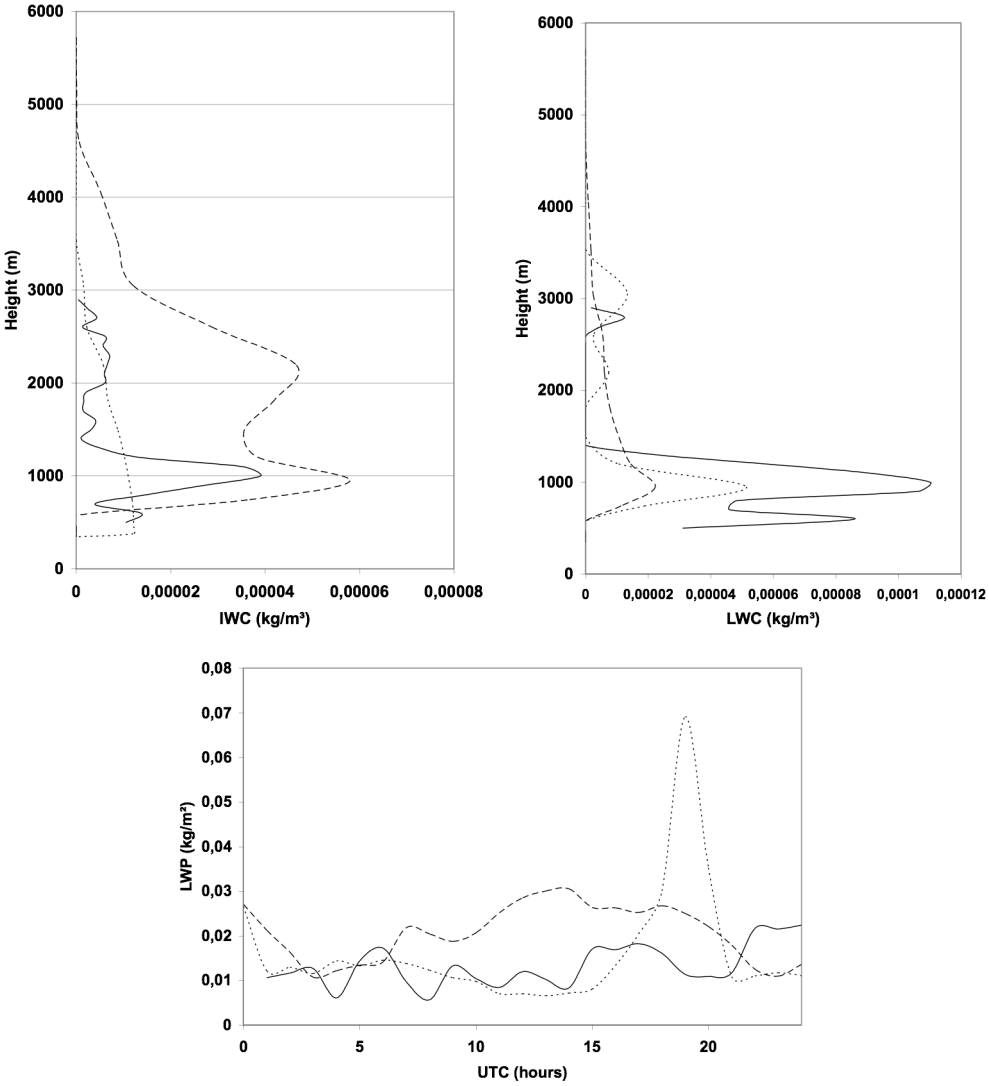

Figure 1: Vertical profile of LWC and IWC and time series of LWP at Oliktuk (modelled vs. observed) for October 8th. Observations (—), SUN results (-----) and KY results (⋯).

Table 1: Time averaged LWP (g m^{-2}) at Oliktok and Atqasuk for October 5th, 6th, 8th and 9th (warm regime) and for October 10th, 12th (cold regime at Atqasuk only)

Regime	Observations	SUN	KY
Warm	56.0	23.2	82.5
Cold	14.0	3.7	17.2

Sundqvist, H., 1978: A parameterization scheme for non-convective condensation including prediction of cloud water content. Quat. J. Roy. Meteor. Soc., 104, 677-690.

Kong, F.-Y and M.K. Yau, 1997: An explicit approach to microphysics in MC2. Atmos. Oc., 35, 257-291.

Shupe, M.D., T.S. Matrasov and T. Uttal, 2006: Arctic mixed-phase cloud properties derived from surface-based sensors at SHEBA. J. Atmos. Sc., 63, 697-711.

Performance of the improved Mellor-Yamada Level 3 scheme on JMA-NHM

Tabito Hara[1]

Numerical Prediction Division, Japan Meteorological Agency,
1-3-4, Otemachi, Chiyoda-ku, Tokyo 100-8122, Japan

1 Introduction

The Japan Meteorological Agency (JMA) has been developing a non-hydrostatic model, which is called JMA-NHM, for operational and research purpose. The model with 5-km horizontal resolution (MSM) is employed for the operational mesoscale numerical prediction which aims at providing the information to prevent disaster(Saito et al. 2007).

In May 2007, the model was replaced by a new one in which implemented physics included the improved Mellor-Yamada Level 3 scheme (Nakanishi and Niino 2004)(MYNN3) and the partial condensation scheme (Sommeria and Deardorff 1977), which have brought considerable improvement. The new model can predict more suitable boundary layer and reduce the negative bias of shortwave radiation flux toward surface(Hara 2007).

In this report, the performance of MYNN3 will be shown through an example of prediction for the case of the mixed layer generated on the Sea of Japan in winter. Compared with the former turbulence scheme of JMA-NHM, based on the eddy-diffusive model (Deardorff 1980) with non-local like effect (Sun and Chang 1986), height of mixed layer is higher and structure of wind in the mixed layer can be well realized.

2 Impact on mixed layer on the Sea of Japan in winter

In winter, mixed layer is often developed on the Sea of Japan because the continental cold air is advected to on the warm sea surface, where cloud are observed to streak along the wind direction from the northwest to the southeast. When cold advection is strong enough to cross the Japan island, mixed layer is also seen on the Pacific Ocean. The typical case is shown in Fig.1, which includes the observation by MTSAT-1R satellite and the simulated satellite images with the predicted quantities of the model with MYNN3, and the one with the previous turbulent scheme based on the eddy diffusive model. Attention should be drawn to the representation of cloud on the Sea of Japan and the Pacific Ocean. Detailed cloud structures can be observed in the image simulated by the model with MYNN3. With the eddy diffusive model, cloud spreads excessively wider. It is because vapor is concentrated as a result of the suppression of its vertical diffusion, and then more cloud is generated due to condensation, which is supported by Fig.2, or the cross section of relative humidity.

A remarkable difference between the results of the model with MYNN3 and the one with the eddy diffusive model can be seen in the vertical profile of wind velocity. Fig.3 shows the cross section of potential temperature and the wind velocity along the line crossing the Sea of Japan. The uniformly diffused distribution, which characterizes mixed layer, is realized for the potential temperature by both of schemes, but as for the wind velocity, horizontal contours come into sight with the eddy diffusive model while uniform wind velocity are seen with MYNN3. It means that vertical transportation of momentum with the eddy diffusive model is not large enough to generate uniform mixed layer which should be generated under this environment.

The difference is made by the order of closure. MYNN3 is based on the second order closure while the eddy diffusive model has the first order closure. In the first order closure model, an eddy diffusive coefficient is determined by the product of square root of turbulent kinetic energy, mixed length, and a proportional constant, which is usually set to 0.1 - 0.2. On the other hand, in the second order closure model, the proportional constant in the first order one is no longer a constant; a variable which depends on environmental field, and it ranges about 1 - 2 under unstable layer, much larger than the value of 0.1 - 0.2 in the first order model. It can provide larger diffusive coefficients which make the turbulence diffusion more active.

3 Concluding Remarks

It has been confirmed that MYNN3 is superior to the previous eddy diffusive model through the example of prediction. The superiority of MYNN3 is demonstrated also through the other cases and statistical verification against observations of sondes and wind profilers.

References

Deardorff, J.W., 1980: Stratocumulus-capped mixed layers derived from a three-dimensional model. *Bound.-Layer Meteor.*, **18**, 495–527.

Hara, T., 2007: Implementation of improved Mellor-Yamada Level 3 scheme and partial condensation scheme to JMANHM and their performance. *CAS/JSC WGNE Res. Activ. Atmos. Oceanic Modell.*, **37**, 0407–0408.

Nakanishi, M. and H. Niino, 2004: An improved Mellor-Yamada level 3 model with condensation physics : Its design and verification. *Bound.-Layer Meteor.*, **112**, 1–31.

Saito, K., J. Ishida, K. Aranami, T. Hara, T. Segawa, M. Narita, and Y. Honda, 2007: Nonhydrostatic Atmospheric Models and Operational Development at JMA. *J. Meteor. Soc. Japan*, **85B**, 271–304.

Sommeria, G. and J.W. Deardorff, 1977: Subgrid-Scale Condensation in Models of Nonprecipitating Clouds. *J. Atmos. Sci.*, **34**, 344–355.

Sun, W. Y. and C. Z. Chang, 1986: Diffusion model for a convective layer. Part I: Numerical simulation of convective boundary layer. *J. Climate Appl. Meteor.*, **25**, 1445–1453.

[1]E-mail: tabito.hara@met.kishou.go.jp

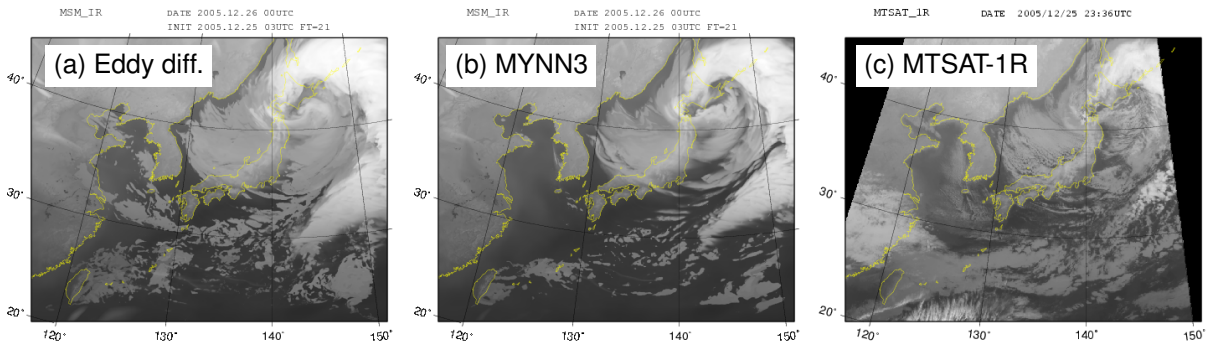

Fig. 1: Simulated IR channel satellite images with predicted quantities and observed image at 0000UTC Dec. 26 2005. (a) simulated image at T+21h with the eddy diffusive model, (b) the same as (a) but with MYNN3, (c) corresponding observed image.

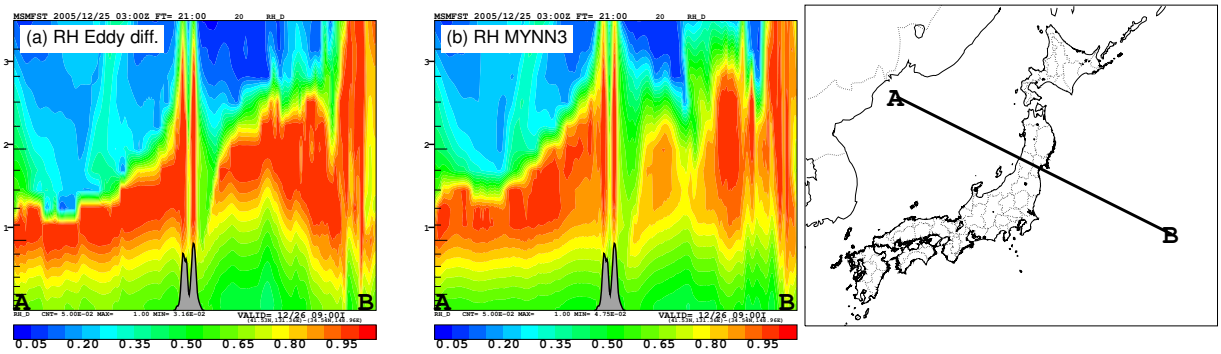

Fig. 2: Cross section of predicted relative humidity along the line AB in the right figure at 0000UTC Dec. 26 2005. Its initial time is 0300 UTC Dec. 25 2005. (a) with the eddy diffusive model, (b) the same as (a) but with MYNN3.

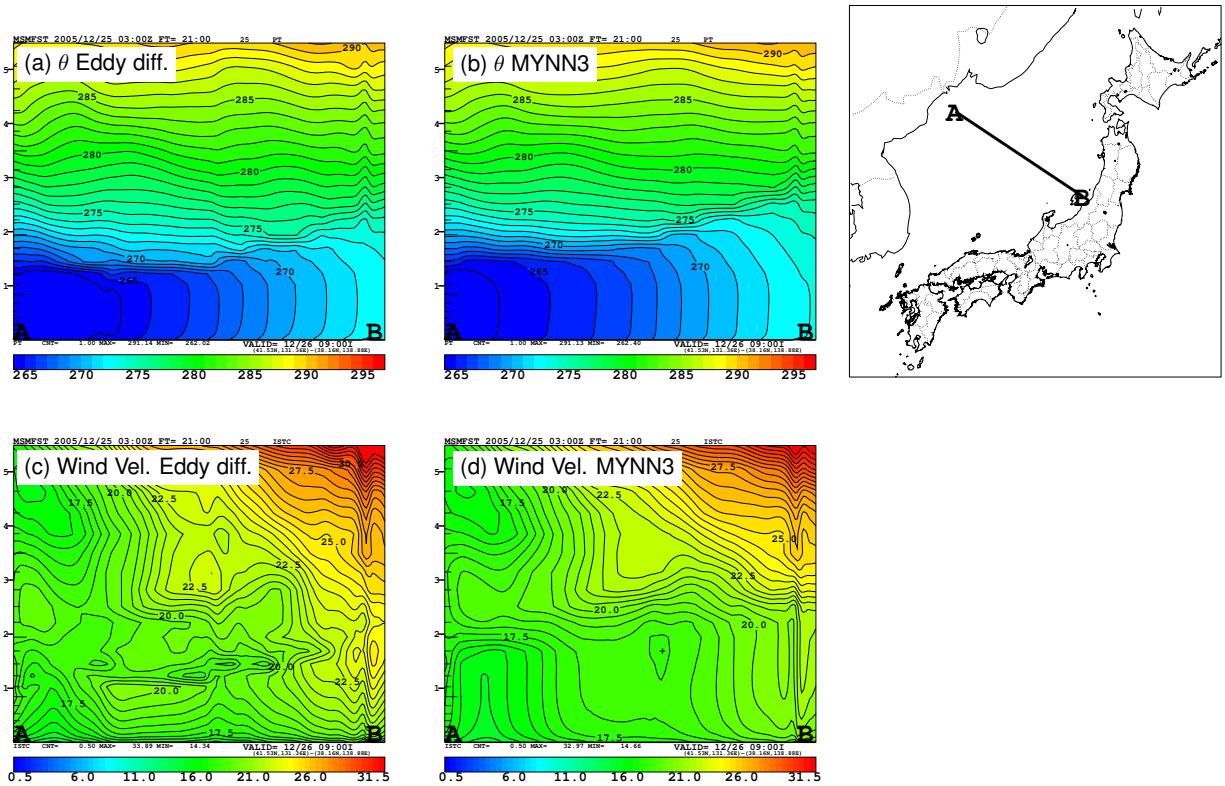

Fig. 3: Cross section of predicted potential temperature and wind velocity along the line AB in the upper-right figure at 0000 UTC Dec. 26 2005. Its initial time is 0300 UTC Dec. 25 2005. (a) potential temperature with the eddy diffusive model, (b) the same as (a) but with MYNN3, (c) wind velocity with the eddy diffusive model, (d) the same as (c) but with MYNN3.

Problems on the usage of Kain-Fritsch parameterization in a 5km model: Statistical comparison with cloud-top heights of cumulonimbi simulated by a cloud resolving model

Teruyuki KATO* and Syugo HAYASHI*

*Meteorological Research Institute / Japan Meteorological Agency, 1-1 Nagamine, Tsukuba, Ibaraki 305-0052, Japan

The major index to estimate cloud-top heights of moist convection (CTOPs) is the level of neutral buoyancy (LNB). Kato et al. (2007) showed that during the Baiu season the vertical profile of the appearance rates of LNB have two peaks at the middle level (~ 700 hPa) and the upper level (~ 200 hPa). These results are statistically obtained from objective analysis data with the horizontal resolution (dx) of 20 km, produced by the Japan Meteorological Agency (JMA). The major purpose of this study is to statistically examine the relationship between the LNB and the CTOPs simulated by a cloud-resolving model with dx = 1 km (1km-CRM). Moreover, in order to clarify the contribution of moist convection to total rainfall amount, the rainfall amount is also statistically estimated according to CTOPs of moist convection. Further, the results of 5-km nonhydrostatic model (5km-NHM) are compared with those of 1km-CRM to study problems on precipitation processes, especially cumulus parameterization.

Numerical models used in this study are the JMA-nonhydrostatic model (JMA-NHM, Saito et al., 2006). The same dynamical and physical processes but for the precipitation and atmospheric boundary layer are used in both models: In the 1km-CRM, a bulk-type microphysics scheme predicting the specific humidity of cloud water q_c, cloud ice q_{ci}, rainwater q_r, snow q_s, and graupel q_g are used, while a moist convection parameterization scheme (Kain and Fritsch, 1990) is additionally used in the 5km-NHM. As for the atmospheric boundary layer processes, the 1km-CRM predicts the turbulent energy, while the 5km-NHM prognostically estimates the turbulence energy and incorporates a mixing length formulation that supports a realistic boundary layer growth. The initial and boundary conditions of the 5km-NHM are produced from JMA objective analysis data with dx = 10 km that are available 3-hourly. The initial times of the 5km-NHM are 00 UTC, 06 UTC, 12 UTC and 18 UTC between 1 May and 31 July 2007, while those of the 1km-CRM are simply interpolated from the 3-h forecasts of the 5km-NHM. The hourly data between 4-h (7-h) and 9-h (12-h) forecasts of the 1km-CRM (5km-NHM) are used in this study.

CTOPs and cloud-bottom heights (CBTMs) are determined by the threshold values of $q_c + q_{ci} + q_s$ = 0.01 g kg^{-1} and that of $q_c + q_{ci}$ = 0.1 g kg^{-1}, respectively. Cumulonimbi are defined as the moist convection with rainfall in this study. The following conditions for their judgment are used; 1) the distance from the ground to CTOP > 2 km, 2) the distance from the ground to CBTM < 2.5 km, 3) the distance between CTOP and CBTM > 1 km, and 4) vertically-integrated $q_r + q_s + q_g$ below a 5-km height ≥ 0.1 mm in the case of CTOP < 8 km. Noted that the location of CTOP may be different from that of CBTM, due to the tilting of cumulonimbi. The difference of vertical scales of cumulonimbi is accepted in this study. The rainfall amount is estimated as follows. The vertically-integrated amount of q_r below a 2-km height is calculated, and the averaged q_r is estimated from it. Then, the terminal velocity of rainwater is estimated from the averaged q_r to obtain the hourly rainfall intensity.

Figure 1 shows the appearance rate distributions of LNB and CTOP of simulated cumulonimbi. The LNB appears at almost a half rate (50 %), while the highest appearance rate of CTOPs is at most 10 % even on the land. These statistical results agree with those of Kato et al. (2007) and Kato (2005). Moreover, the appearance rates of CTOPs are relatively higher on the land than over the sea, while those of LNB have opposite features. Terrain-induced updrafts often lift a low-level air to the LFC, and consequently higher appearance rates of CTOPs can be produced on the land. Further, CTOPs are overestimated on the land and underestimated over the sea by the 5km-NHM.

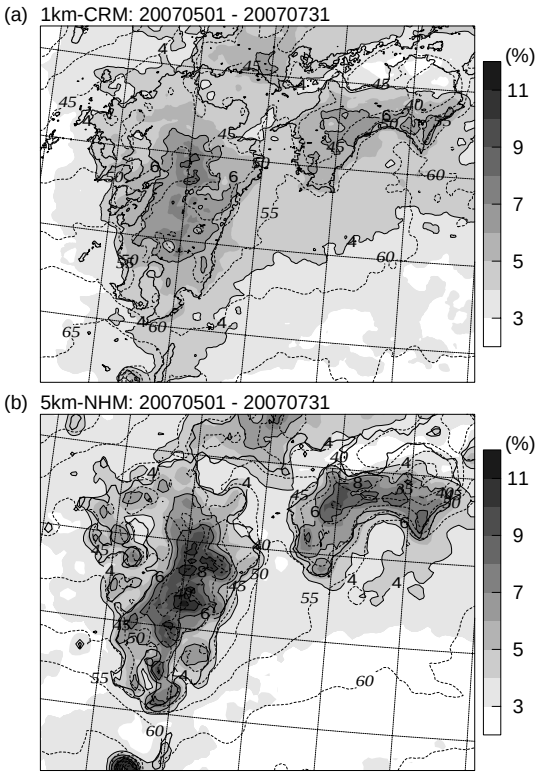

Fig. 1 Appearance rates of CTOP (shade) and LNB (dashed contours), averaged between 1 May and 31 July 2007, estimated by the (a) 1km-CRM and (b) 5km-NHM.

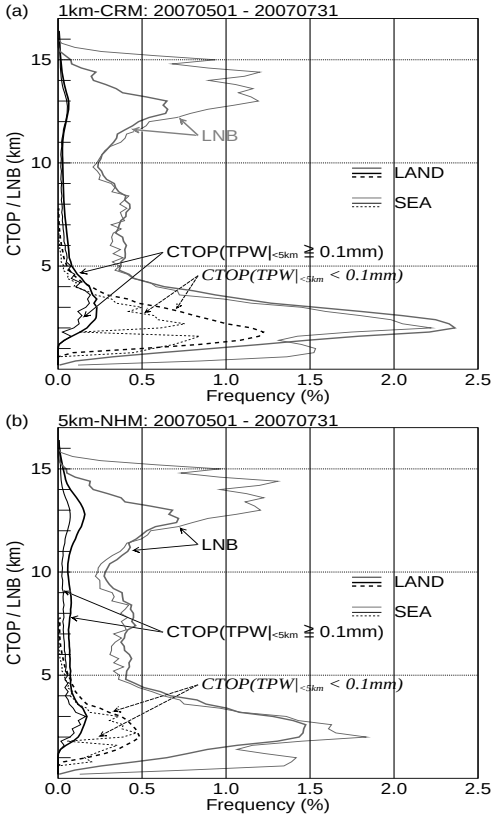

Fig. 2 Vertical profiles of appearance frequencies of LNB (grey lines) and CTOP (solid lines), averaged between 1 May and 31 July 2007, estimated by the (a) 1km-CRM and (b) 5km-NHM. Dashed lines denote the results for CTOPs with vertically-integrated total amount of rainwater, snow and graupel (TPW) below a height of about 5 km < 0.1 mm. Thick and thin lines present the results on the land and over the sea, respectively. Each frequency is calculated by dividing heights into 80 levels with an interval of 200 m.

Two vertical peaks appear in the appearance rates of the LNB estimated from the simulation results (grey lines in Fig. 2), as well as Kato et al. (2007). Any remarkable differences are not found between the LNB profiles of 1km-CRM and 5km-NHM. Meanwhile, two peaks also appear in the vertical profile of the appearance rates of simulated CTOPs (solid lines). The rates at the top peak around 13 km are less than 10 % of those of the LNB. The appearance rates for CTOPs not to satisfy the condition 4) for judging cumulonimbi (dashed lines) have a peak around a 2-km height, and the rates corresponding to the peak are about a half of those of the LNB. Such CTOPs could form associated with the cumulus and cumulus congestus. Moreover, the 5km-NHM overdevelops cumulonimbi, especially on the land, while the moist convection formed corresponding to the lower LNB appears at about a half rate in comparison with that simulated by the 1km-CRM.

The contribution rate of cumulonimbi, defined in this study, to total rainfall amount is about 70 % both over the sea and on the land (not shown). The vertical profile of the contribution rates on the land, estimated from the results of 1km-CRM, show that in June and July the maximum contribution rate is brought from cumulonimbi with a CTOP of 3 ~ 4 km (Fig. 3a). In May, the contribution rate associated with such cumulonimbi is as large as that found at the upper level of about 12 km. These results mean that slight numbers of developed cumulonimbi with a CTOP exceeding 10 km (see Fig. 2) produce considerably large rainfall amount, while about a half of total rainfall amount is produced by cumulonimbi with a CTOP lower than 5 km. In comparison with the results of 1km-CRM (Fig. 3a), the 5km-NHM (Fig. 3b) overestimates the contribution of developed cumulonimbi, and it underestimates that of the moist convection formed corresponding to the lower LNB independent of the seasonal change. Moreover, in May and June another peak is found around a height of 7-9 km. This could be brought from the over-development of cumulonimbi with a CTOP lower than 5 km by using the Kain-Fritsch convective parameterization scheme.

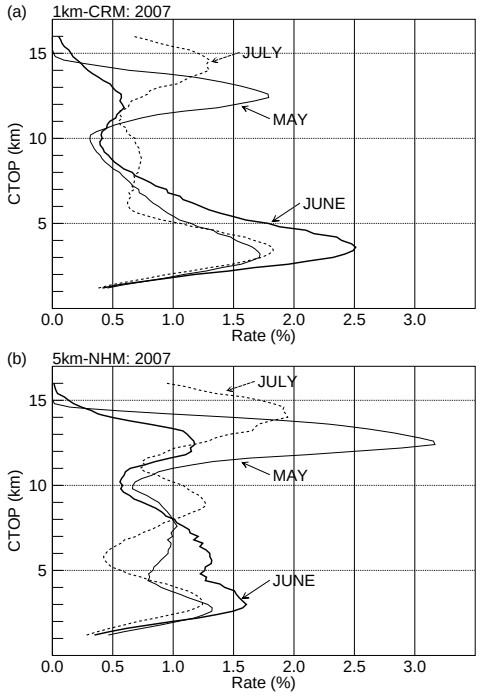

Fig. 3 Same as Fig. 2, but for the seasonal change of contribution rates to total rainfall amount according to CTOPs on the land.

REFERECES

Kain, J. S. and J. M. Fritsch, 1990: A one-dimensional entraining/detraining plume model and its application in convective parameterization. J. Atmos. Sci., 47, 2784-2802.

Kato, T., 2005: Statistical study of band-shaped rainfall systems, the Koshikijima and Nagasaki lines, observed around Kyushu Island, Japan, *J. Meteor. Soc. Japan*, **83**, 943-957.

Kato, T., S. Hayashi, and M. Yoshizaki, 2007: Statistical study on cloud top heights of cumulonimbi thermodynamically estimated from objective analysis data during the Baiu season, *J. Meteor. Soc. Japan*, **85**, 529-557.

Saito, K, T. Fujita, Y. Yamada, J. Ishida, Y.Kumagai, K. Aranami, S. Ohmori, R. Nagasawa, S. Kumagai, C. Muroi, T. Kato, H. Eito, and Y. Yamazaki, 2006: The Operational JMA Nonhydrostatic Mesoscale Model, *Mon. Wea. Rev.*, **134**, 1266-1297.

Improvement of the Cumulus Parameterization Scheme of the Operational Global NWP Model at JMA

Masayuki Nakagawa

Numerical Prediction Division, Japan Meteorological Agency

1-3-4 Otemachi, Chiyoda-ku, Tokyo 100-8122, JAPAN

m-nakagawa@met.kishou.go.jp

The cumulus parameterization scheme implemented in the operational Global Spectral Model (GSM) at the Japan Meteorological Agency (JMA) follows the scheme proposed by Arakawa and Schubert (1974) with modifications by Moorthi and Suarez (1992), Randall and Pan (1993) and Pan and Randall (1998). The convection triggering mechanism proposed by Xie and Zhang (2000), dynamic CAPE generation rate (DCAPE), is introduced to improve the rainfall forecast (Nakagawa 2005).

JMA revised the calculation procedure of DCAPE for the operational GSM in January 2008 to consider the effect of wind crossing the isobar at the surface more precisely, which is not taken into account sufficiently in the previous version. An excessive limitation on cumulus upward mass flux from redundant vertical CFL condition was also removed.

The effect of the revision on DCAPE calculation appears mainly in forecasts of orographic precipitation. Figure 1 shows 6-hour accumulated precipitation at 12UTC 18 August 2006 by the forecasts with the previous GSM (left) and the current GSM (center) and by the radar observation (right). Typhoon T0610 (WUKONG) was moving northward over Kyusyu Island (big island in the center of the figure) and heavy precipitation occurred in the western part of Japan. Strong southerly wind was observed around the east side of the typhoon. It can be seen that the peak of rainfall near the Shikoku Island (the island east of

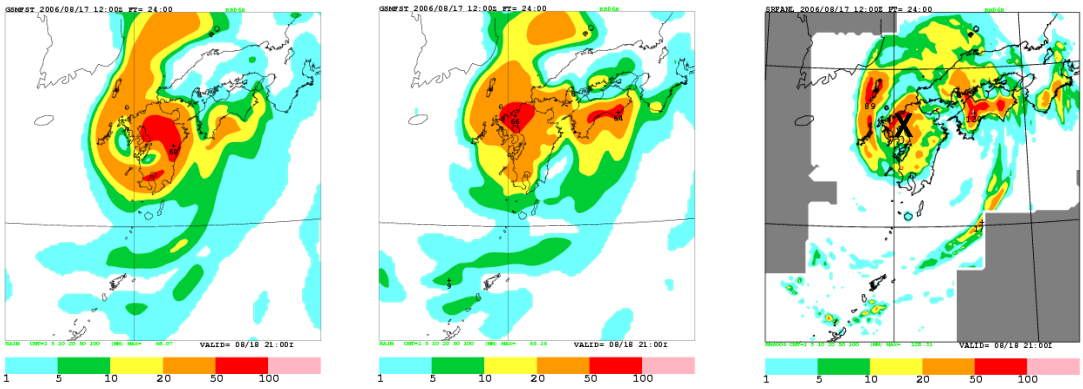

Fig. 1. Six-hour accumulated precipitation at 12UTC 18 August 2006 by the forecasts with the previous GSM (left) and the current GSM (center) and by the radar observation (right). Initial time for forecasts is 12 UTC 17 August 2006. X in the right panel indicates the position of typhoon T0610 (WUKONG).

Kyusyu Island) is predicted over the sea by the previous GSM. On the other hand, the current GSM simulates the peak over the Shikoku Island, which agrees better with the observation. The heavy precipitation over the Kyusyu Island is also predicted more appropriately by the current GSM.

Figure 2 shows the equitable threat scores for 6-hour accumulated precipitation forecasts against the raingauge observation over Japan in August 2006. The score of the current GSM is superior to that of the previous one.

The mean positional errors of the typhoons track forecast in August 2006 are shown in Figure 3. We can see that the revision of the cumulus parameterization scheme reduced the typhoon positional error substantially.

References.

Arakawa, A. and W. H. Schubert, 1974: Interaction of a cumulus cloud ensemble with the large-scale environment, Part I. *J. Atmos. Sci.*, **31**, 674-701.

Moorthi, S. and M. J. Suarez, 1992: Relaxed Arakawa-Schubert: A parameterization of moist convection for general circulation models. *Mon. Wea. Rev.*, **120**, 978-1002.

Nakagawa, M., 2005: Precipitation forecasts by a high resolution global model at JMA. *BMRC research report No. 111*, 127-130.

Pan, D.-M. and D. Randall, 1998: A cumulus parameterization with a prognostic closure. *Quart. J. Roy. Meteor. Soc.*, **124**, 949-981.

Randall, D. and D.-M. Pan, 1993: Implementation of the Arakawa-Schubert cumulus parameterization with a prognostic closure. *Meteorological Monograph/The representation of cumulus convection in numerical models.*, **46**, 137-144.

Xie, S., C., and M. H. Zhang, 2000: Impact of the convective triggering function on single-column model simulations. *J. Geophys. Res.*, *105*, 14983-14996.

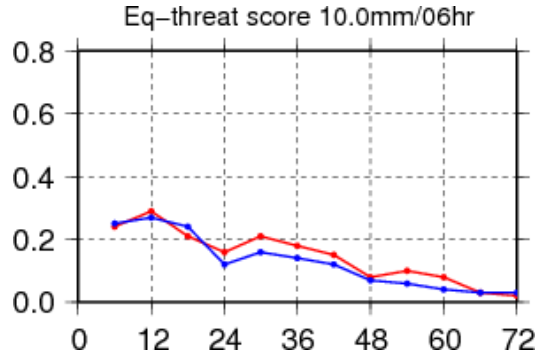

Fig. 2. Equitable threat scores for 6-hour accumulated precipitation forecasts against the raingauge observation over Japan in August 2006 by the current (red) and the previous (blue) GSM. The x-axis denotes the forecast time (hour).

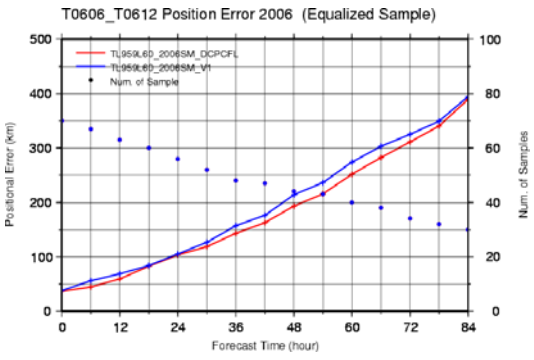

Fig. 3. Mean positional errors of the typhoons track forecast in August 2006. The red and blue line indicates the mean error of the current and the previous GSM, respectively. The dots represent the sample size.

Inclusion of a temperature perturbation based on the relative humidity to the Kain-Fritsch convective parameterization scheme

Masami Narita
Numerical Prediction Division, Japan Meteorological Agency
1-3-4 Otemachi, Chiyodaku, Tokyo 100-8122, Japan
E-mail: m_narita@naps.kishou.go.jp

The Japan Meteorological Agency has operated a nonhydrostatic mesoscale model (MSM) of 5-km grid spacing since March 2006. To represent the effects of subgrid-scale convection, the Kain-Fritsch (KF) convective parameterization scheme (Kain and Fritsch 1990; Kain 2004) is adopted to MSM in addition to cloud microphysics (Ohmori and Yamada 2004). The source codes of the KF scheme have been originally developed for the Weather Research and Forecast (WRF) modeling system and implemented to MSM with Dr. Kain's consent in April 2002. In addition to the minor improvements on the KF scheme in WRF before February 2003, some modifications were applied to the KF scheme in MSM.

To identify source layers for convective clouds, the KF scheme utilizes a trigger function based on the temperature at the lifting condensation level (LCL) and the grid-scale vertical velocity (Kain 2004). The KF scheme, applied to the humid climate area of Japan and its surroundings, sometimes fails to initiate parameterized convection when the lowest atmosphere is wet and dynamical forcing is weak. To eliminate this weakness, a temperature perturbation based on the relative humidity, which was originally developed for the High Resolution Limited Area Model by Undén et al. (2002), has been added to the trigger function. This new temperature perturbation ΔT_{RH} is given by

$$\Delta T_{\mathrm{RH}} = \begin{cases} 0, & \text{if } R_{\mathrm{hLCL}} < 0.75 \\ \dfrac{0.25\left(R_{\mathrm{hLCL}} - 0.75\right) q_{\mathrm{mix}}}{\partial q^{*}_{\mathrm{LCL}} / \partial T}, & \text{if } 0.75 \le R_{\mathrm{hLCL}} \le 0.95 \\ \dfrac{\left(1/R_{\mathrm{hLCL}} - 1\right) q_{\mathrm{mix}}}{\partial q^{*}_{\mathrm{LCL}} / \partial T}, & \text{if } R_{\mathrm{hLCL}} > 0.95 \end{cases}$$

where R_{hLCL} is the relative humidity at the LCL, T is the temperature, q^{*}_{LCL} is the saturation mixing ratio at the LCL, q_{mix} is the mixing ratio of updraft source layer. The temperature perturbation determined by the formulation of Undén et al. (2002) is reduced to a certain degree in MSM.

Figure 1 shows the accumulated precipitation forecasts by MSM. In Fig. 1 (a), without the relative humidity based temperature perturbation, considerably intensified precipitation was generated in very small areas such as the western sea of Taiwan (234 mm/3h), the southern sea of Okinawa island (115 mm/3h) and so on. Such intensified precipitation caused by grid-point storms was eliminated with the modified KF scheme as

shown in Fig. 1 (b).

The inclusion of the temperature perturbation depending on the relative humidity also improved the forecast of diurnal convective rain (Fig. 2). While the amount of precipitation (b) was not adequate compared to the observation (a), the predicted precipitation pattern calculated by the modified KF scheme (c) was better than that by the KF scheme without the relative humidity based temperature perturbation.

References

Kain, J. S., 2004: The Kain-Fritsch convective parameterization: An update. *J. Appl. Meteor.*, **43**, 170-181.

Kain, J. S., and J. M. Fritsch, 1990: A one-dimensional entraining/detraining plume model and its application in convective parameterization. *J. Atmos. Sci.*, **47**, 2784-2802.

Ohmori, S. and Y. Yamada, 2004: Implementation of the Kain-Fritsch convective parameterization scheme in the JMA's non-hydrostatic model. *CAS/JSC WGNE Research Activities in Atmospheric and Oceanic Modelling*, **34**, 0425-0426.

Undén, P., L Rontu, H Järvinen, P. Lynch, J. Calvo, G. Cats, J. Cuxart, K. Eerola, C. Fortelius, J. A. Garcia-Moya, C. Jones, G. Lenderlink, A. McDonald, R. McGrath, B. Navascues, N. W. Nielsen, V Ødegaard, E. Rodriguez, M. Rummukainen, R. Rõõm, K. Sattler, B. H. Sass, H. Savijärvi, B. W. Schreur, R. Sigg, H. The, A. Tijm, 2002: *HIRLAM-5 Scientific Documentation*, 144 pp.

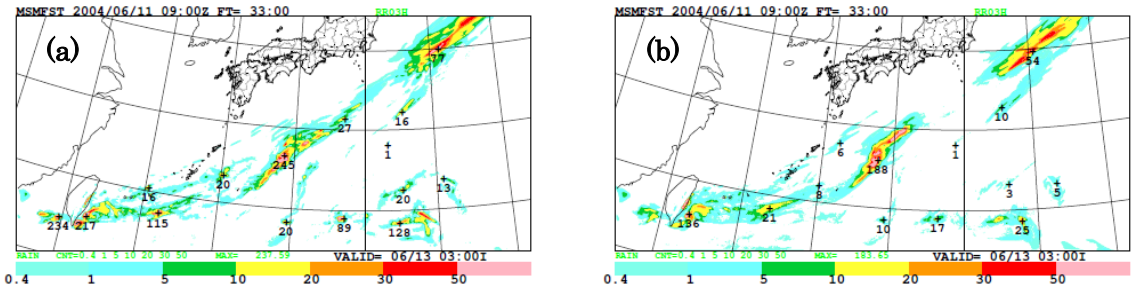

Fig. 1. Accumulated precipitation [mm/3h] from 15-18 UTC on 12th June 2004.
(a) 33-hour forecast by MSM with the KF scheme without the relative humidity based temperature perturbation.
(b) Same as (a) but with the relative humidity based temperature perturbation.

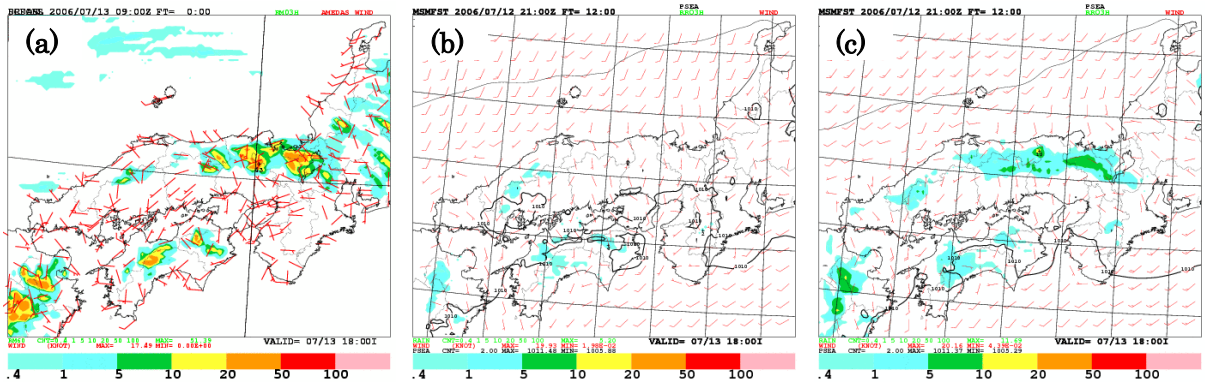

Fig. 2. Accumulated precipitation [mm/3h] from 06-09 UTC on 13th July 2006.
(a) Observation (derived from radar data corrected by rain gauge data).
(b) 33-hour forecast by MSM with the KF scheme without the relative humidity based temperature perturbation.
(c) Same as (b) but with the relative humidity based temperature perturbation.

Improved numerical scheme of turbulence closure.

V.Shnaydman, G.Stenchikov
Department of Environmental Science, Rutgers-The State University of NJ, USA
Email: volf@envsci.rutgers.edu, gera@envsci.rutgers.edu

We developed an improved numerical scheme for solution of turbulence closure equations and demonstrate its effectiveness applying it to the one-dimensional non-stationary atmospheric boundary layer (ABL). The two-equation closure scheme includes the equations of turbulent kinetic energy (1) and dissipation rate (2) along with Kolmogorov-Prandtl relationship for the turbulence coefficient (3) [Shnaydman, Berkovich].

$$\frac{\partial E}{\partial t} = k\left[\left(\frac{\partial u}{\partial z}\right)^2 + \left(\frac{\partial v}{\partial z}\right)^2\right] - \alpha_T k \frac{g}{\theta_0}\frac{\partial \theta}{\partial z} + \alpha_\varepsilon \frac{\partial}{\partial z} k \frac{\partial E}{\partial z} - \varepsilon \qquad (1)$$

$$\frac{\partial \varepsilon}{\partial t} = \frac{\varepsilon}{E}\left\{\alpha_1 k\left[\left(\frac{\partial u}{\partial z}\right)^2 + \left(\frac{\partial v}{\partial z}\right)^2\right] - \alpha_2 k \frac{g}{\theta_0}\frac{\partial \theta}{\partial z} - \alpha_3 \varepsilon\right\} + \alpha_4 \frac{\partial}{\partial z} k \frac{\partial \varepsilon}{\partial z} \qquad (2)$$

$$k = \alpha_\varepsilon \frac{E^2}{\varepsilon} \qquad (3)$$

Nowadays the two-equation turbulence closure became a standard feature of many ABL models. So it is important to develop adequate numerical algorithms for solution equations (1-3). This algorithm has to be numerically stable for relatively large time steps and positively defined for turbulence kinetic energy (TKE) and dissipation. Unfortunately in many ABL models the fulfillment of these requirements depends on relations between the mechanisms of ABL formation especially between the TKE production and the effect of the buoyancy force [Jiang]. This in some cases could produce erroneous results. Therefore here we developed a finite-difference scheme for (1-3) that is numerically stable and keeps TKE and ε positive throughout entire integration.

We conducted numerical experiments to choose the most suitable form for the non-linear and buoyancy terms. First we realized that linearization of square terms on one time step has to be done in the following way ($\varphi = (E, \varepsilon)$, φ and φ^n are the values of unknown variables at given time t and at the previous time step):

$$\varphi^2 = 2\varphi \times \varphi^n - (\varphi^n)^2 \qquad (4)$$

Then we multiply the buoyancy term by δ for stable stratification when δ =1 and by 1-δ for unstable stratification when δ =0.

Using these relations we rewrite the TKE and dissipation equations in the following form:

$$\frac{\partial E}{\partial t} + (2\alpha_T \alpha_\varepsilon \delta \times \frac{g}{\theta_0}\frac{\partial \theta}{\partial z} \times \frac{E^n}{\varepsilon^n}) \times E - \frac{\partial}{\partial z} k \frac{\partial E}{\partial z} + \varepsilon = F_E^n \quad (5)$$

$$\frac{\partial \varepsilon}{\partial t} + (2\alpha_2 \alpha_T \alpha_\varepsilon \delta \times \frac{g}{\theta_0}\frac{\partial \theta}{\partial z}) \times E - 2\alpha_3 \frac{\varepsilon^n}{E_n} \times \varepsilon - \alpha_4 \frac{\partial}{\partial z} k \frac{\partial \varepsilon}{\partial z} = F_\varepsilon^n \quad (6)$$

$$F_E^n = k_n \left[(\frac{\partial u}{\partial z})^2 + (\frac{\partial v}{\partial z})^2 + (2\delta - 1)\alpha_T \frac{g}{\theta_0}\frac{\partial \theta}{\partial z} \right] \quad (7)$$

$$F_\varepsilon^n = \alpha_\varepsilon E^n \left[\alpha_1 \left((\frac{\partial u}{\partial z})^2 + (\frac{\partial v}{\partial z})^2 \right) - (1 - \delta)\alpha_2 \frac{g}{\theta_0}\frac{\partial \theta}{\partial z} \right] + \alpha_3 \frac{(\varepsilon^n)^2}{E^n} \quad (8)$$

The finite difference equations were obtained using first-order approximation in time, and centered-in-space differences for the vertical turbulent terms (second-order approximation in space). The implicit numerical integration scheme was applied. This scheme is used here for the stationary problem:

$$a_1 E_{m-1} - a_2 E_m + a_3 E_{m+1} + \varepsilon_m = (F_E^n)_m \delta t + E_m^n \quad (9)$$

$$b_1 \varepsilon_{m-1} - b_2 \varepsilon_m + b_3 \varepsilon_{m+1} + b_4 E_m = (F_\varepsilon^n)_m \delta t + \varepsilon_m^n \quad (10)$$

Now we can re-write the system (9-10) in matrix form:

$$A W_{m-1} - B W_m + C W_{r+1} = D_m \quad (11)$$

Equation (11) was solved numerically using factorization method. The conditions of stability and positive solution were fulfilled independently and turbulent kinetic energy and dissipation rate were kept positive for all conditions.

Reference

Shnaydman V., Berkovich L. 2006 Atmospheric boundary modeling in numerical prediction operations. Research Activity in Atmospheric and Oceanic Modeling, 5-57

Jiang W, Zhou M, Xu M et al (2002) Study on development and application of a regional PBL numerical model. Boundary-Layer Meteorol 104: 491-503